Endothelium-targeted overexpression of heat shock protein 27 ameliorates blood–brain barrier disruption after ischemic brain injury

Yejie Shi[a,b,c,1], Xiaoyan Jiang[a,c,1], Lili Zhang[b,c], Hongjian Pu[c], Xiaoming Hu[a,b,c], Wenting Zhang[a], Wei Cai[c], Yanqin Gao[a,c], Rehana K. Leak[d], Richard F. Keep[e], Michael V. L. Bennett[a,f,2], and Jun Chen[a,b,c,2]

[a]State Key Laboratory of Medical Neurobiology, Institute of Brain Sciences and Collaborative Innovation Center for Brain Science, Fudan University, Shanghai 200032, China; [b]Geriatric Research, Education and Clinical Center, Veterans Affairs Pittsburgh Healthcare System, Pittsburgh, PA 15261; [c]Pittsburgh Institute of Brain Disorders & Recovery and Department of Neurology, University of Pittsburgh, Pittsburgh, PA 15213; [d]Division of Pharmaceutical Sciences, Mylan School of Pharmacy, Duquesne University, Pittsburgh, PA 15282; [e]Department of Neurosurgery, University of Michigan, Ann Arbor, MI 48109; and [f]Dominick P. Purpura Department of Neuroscience, Albert Einstein College of Medicine, Bronx, NY 10461

Contributed by Michael V. L. Bennett, December 23, 2016 (sent for review October 10, 2016; reviewed by Johannes Boltze, Cesario Borlongan, and Ke Jian Liu)

The damage borne by the endothelial cells (ECs) forming the blood–brain barrier (BBB) during ischemic stroke and other neurological conditions disrupts the structure and function of the neurovascular unit and contributes to poor patient outcomes. We recently reported that structural aberrations in brain microvascular ECs—namely, uncontrolled actin polymerization and subsequent disassembly of junctional proteins, are a possible cause of the early onset BBB breach that arises within 30–60 min of reperfusion after transient focal ischemia. Here, we investigated the role of heat shock protein 27 (HSP27) as a direct inhibitor of actin polymerization and protectant against BBB disruption after ischemia/reperfusion (I/R). Using in vivo and in vitro models, we found that targeted overexpression of HSP27 specifically within ECs—but not within neurons—ameliorated BBB impairment 1–24 h after I/R. Mechanistically, HSP27 suppressed I/R-induced aberrant actin polymerization, stress fiber formation, and junctional protein translocation in brain microvascular ECs, independent of its protective actions against cell death. By preserving BBB integrity after I/R, EC-targeted HSP27 overexpression attenuated the infiltration of potentially destructive neutrophils and macrophages into brain parenchyma, thereby improving long-term stroke outcome. Notably, early poststroke administration of HSP27 attached to a cell-penetrating transduction domain (TAT-HSP27) rapidly elevated HSP27 levels in brain microvessels and ameliorated I/R-induced BBB disruption and subsequent neurological deficits. Thus, the present study demonstrates that HSP27 can function at the EC level to preserve BBB integrity after I/R brain injury. HSP27 may be a therapeutic agent for ischemic stroke and other neurological conditions involving BBB breakdown.

endothelial cell | stress fiber | tight junction | neuroinflammation | HSP27

The blood–brain barrier (BBB) is a unique microvascular structure in the brain that helps to control the passage of material between blood and brain and maintain the homeostatic microenvironment for normal neuronal functions (1). When BBB integrity is compromised in disease or injury states, proinflammatory factors produced within the injured brain may cross the BBB to attract circulating immune cells, and immune cells, pathogens, and toxins in the blood may penetrate the brain parenchyma and elicit a secondary injury cascade (1). Following cerebral ischemia/reperfusion (I/R), BBB breakdown may produce severe clinical consequences, such as vasogenic brain edema and hemorrhagic transformation, leading to poor neurological outcomes and limiting the use of tissue plasminogen activator (tPA) thrombolysis (2, 3). Therefore, it is necessary to develop effective therapeutic strategies that protect BBB integrity and prevent permanent neurovascular injury after I/R. Treatments that preserve the structure of the BBB would mitigate diffusion of deleterious mediators from blood to brain and from brain to blood.

Brain capillary endothelial cells (ECs) are tightly connected by apical tight junctions (TJs) that form a barrier to the penetration of hydrophilic molecules between plasma and brain and also by adherens junctions (AJs) that connect the cytoskeletons of adjacent cells (1). In many earlier studies, matrix metalloproteinase (MMP)-mediated degradation of EC junctions and basal lamina was thought to be primarily responsible for all types of BBB breakdown after I/R injury (4–6). However, recent reports have revealed additional, MMP-independent mechanisms at the EC level that act before the frank degradation of junctional proteins after I/R (7–10). For example, increased transcellular vesicular trafficking mediated by caveolin-1 and exocytotic machinery may account for BBB hyperpermeability as early as 6 h after cerebral I/R, well before profound TJ structural deficits are observed at 48 h after I/R (8). Moreover, our recent study (9) identified cytoskeletal alterations in brain ECs as an initiator of BBB rupture at even earlier stages (30–60 min after I/R). Specifically, I/R rapidly triggers robust actin polymerization in ECs through activation of the Rho-associated protein kinase (ROCK)/myosin

Significance

Blood–brain barrier (BBB) breakdown is a catastrophic event in the pathogenesis of various neurological disorders, including stroke. Here we report that overexpressing heat shock protein 27 (HSP27) specifically within microvascular endothelial cells protects the BBB in models of ischemic stroke. HSP27 achieves this protection through a previously unexplored mechanism—the inhibition of actin polymerization—that suppresses early structural changes within endothelial cells that appear to initiate the BBB breach. Furthermore, intravenous delivery of a cell membrane-permeable TAT-HSP27 protein after postischemic reperfusion boosts endothelial HSP27 and improves BBB integrity and long-term functional outcomes. Thus, HSP27 has translational potential as a therapeutic agent to ameliorate BBB disruption, reduce the progression of brain injury, and improve long-term neurological outcomes in stroke victims.

Author contributions: Y.S., M.V.L.B., and J.C. designed research; Y.S., X.J., L.Z., H.P., and W.C. performed research; W.Z. and Y.G. contributed new reagents/analytic tools; Y.S., X.H., R.K.L., R.F.K., M.V.L.B., and J.C. analyzed data; and Y.S., R.K.L., M.V.L.B., and J.C. wrote the paper.

Reviewers: J.B., Fraunhofer Institute for Cell Therapy and Immunology and Fraunhofer Research Institution for Marine Biotechnology; C.B., University of South Florida; and K.J.L., University of New Mexico.

The authors declare no conflict of interest.

[1]Y.S. and X.J. contributed equally to this work.

[2]To whom correspondence may be addressed. Email: michael.bennett@einstein.yu.edu or chenj2@upmc.edu.

This article contains supporting information online at www.pnas.org/lookup/suppl/doi:10.1073/pnas.1621174114/-/DCSupplemental.

light chain (MLC) signal transduction cascade, resulting in the formation of force-generating, contractile stress fibers consisting of F-actin, myosin, and other proteins (9, 11). Possibly as a consequence of tension transmission, at least in part, TJ and AJ proteins that are normally anchored to the actin cytoskeleton are disassembled at cell–cell contacts and internalized (12, 13), thereby widening the paracellular space between ECs. This mild damage renders the BBB more vulnerable to subsequent attack by MMPs and facilitates peripheral leukocyte and macrophage infiltration, eventually leading to permanent neurovascular injury (9). Thus, aberrant actin polymerization in ECs enables this vicious feedforward process and represents a rational therapeutic target for BBB protection after I/R.

Heat shock proteins (HSPs) are molecular chaperones that are highly evolutionarily conserved due to their critical role in the response to stressors. HSP27 is a member of the small HSP family with a monomeric molecular mass of 25 and 27 kDa in mouse and human, respectively (14). Under physiological conditions, the level of HSP27 is extremely low in the brain; however, HSP27 expression is transiently induced in brain glial cells and/or ECs at 24 h or later following cerebral I/R (14). Previous studies by our and other groups demonstrated robust neuroprotective effects of HSP27 overexpression against I/R brain injury (15–18), which were largely credited to its antiapoptotic actions. However, HSP27 exerts additional actions on ECs (14). For example, HSP27 can directly inhibit actin polymerization by capping the barbed end of filamentous actin (F-actin) (19, 20) and by sequestering globular actin (G-actin) (21). Thus, the present study sought to test the hypothesis that HSP27 suppresses I/R-induced early onset BBB leakage through inhibiting actin polymerization and the disassembly of junctional proteins in cerebral ECs. The results show that endothelium-targeted overexpression of HSP27 provides long-lasting protection against I/R-induced BBB disruption and neurological deficits.

Results

EC-Specific Overexpression of HSP27 Ameliorates BBB Disruption After I/R Brain Injury. We previously reported that transgenic mice with ubiquitous overexpression of HSP27 developed significantly less brain damage after cerebral I/R, including less BBB disruption (17, 18, 22). These beneficial effects of HSP27 were attributed mainly to its well-characterized antiapoptotic functions

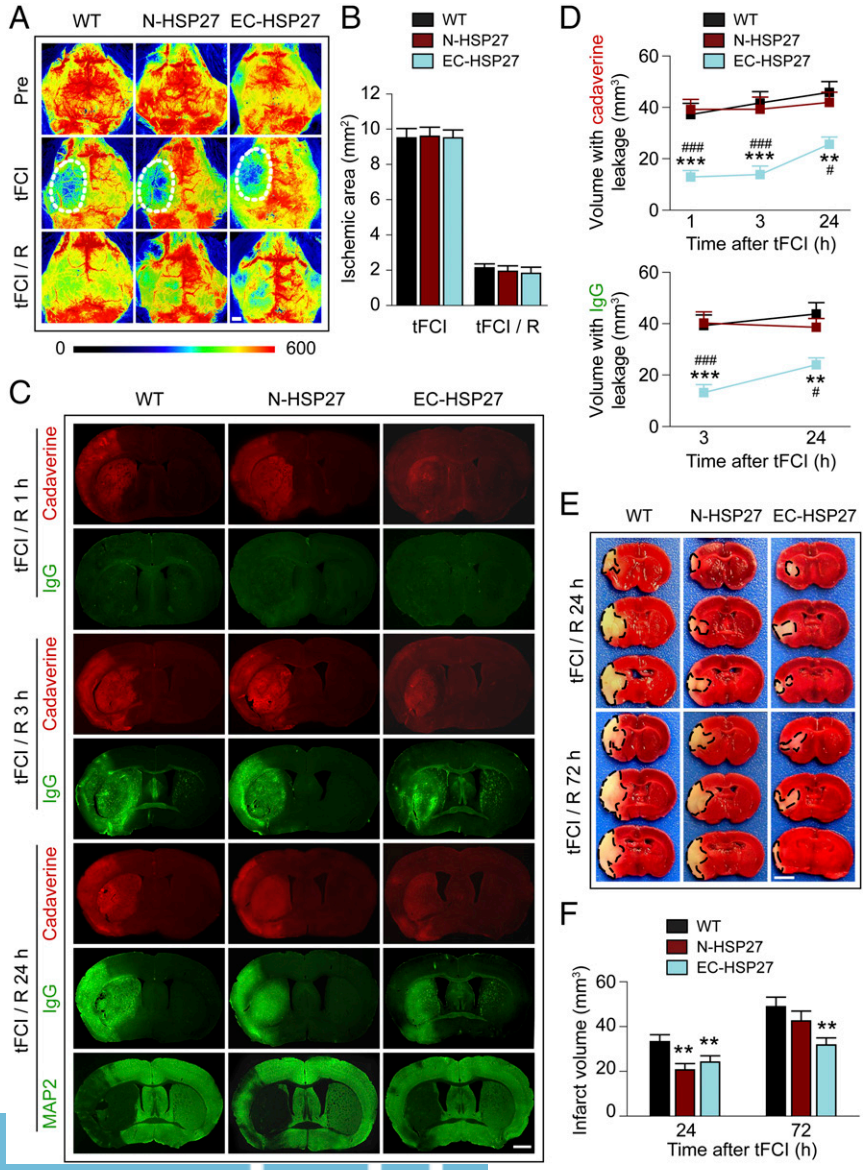

Fig. 1. Targeted overexpression of HSP27 within ECs but not within neurons ameliorates both early and late-onset BBB impairments and I/R brain injury. tFCI was induced for 1 h in WT mice, transgenic mice with neuron-specific HSP27 overexpression (N-HSP27), or transgenic mice with endothelial cell-targeted HSP27 overexpression (EC-HSP27). (*A*) Representative 2D laser speckle images show cortical CBF at 15 min before tFCI (Pre), 15 min after the onset of tFCI, and after 15 min of reperfusion (R). White oval, ischemic area. (Scale bar: 1 mm.) (*B*) Quantitative measurement of ischemic cortical areas by laser speckle imaging after 15 min tFCI and after 15 min poststroke reperfusion (tFCI/R) in WT, N-HSP27, and EC-HSP27 mice. $n = 5$–6 mice per group. Ischemic areas are defined as cortical CBF reduction greater than 65% compared with pre-tFCI CBF levels in the same animals. (*C*) Representative images demonstrate the extravasation of Alexa 555 cadaverine (0.95 kDa, red) or endogenous plasma IgG (~150 kDa, green) into the brain parenchyma 1, 3, or 24 h after 1-h tFCI. At 24 h after tFCI, the area with loss of microtubule-associated protein 2 (MAP2) immunofluorescence illustrates the infarct zone on adjacent sections from the same brains. (Scale bar: 1 mm.) (*D*) Volume of the brain with leakage of cadaverine and IgG at indicated time of reperfusion after tFCI. $n = 6$ mice per group. (*E* and *F*) Brain infarct volume at 24 and 72 h after tFCI was measured on TTC-stained coronal sections. Dashed line, infarct. (Scale bar: 2 mm.) $n = 6$–8 mice per group. $^{**}P \leq 0.01$, $^{***}P \leq 0.001$ vs. WT. $^{\#}P \leq 0.05$, $^{\#\#\#}P \leq 0.001$ vs. N-HSP27.

in neurons (17, 18) and ECs (22). However, neuronal, glial, or endothelial HSP27 may have distinct effects on the pathogenesis of I/R brain injury, which would not be distinguishable in global HSP27-overexpressing mice. Although HSP27 has been shown to attenuate EC apoptosis and TJ degradation at 24 h after I/R (22), whether HSP27 affects the integrity of the BBB at earlier stages is unknown. To elucidate the specific role of HSP27 in various cell types after I/R, we generated transgenic mice overexpressing HSP27 specifically in neurons (N-HSP27; Fig. S1*A*) or in ECs (EC-HSP27; Fig. S1*C*). HA-tagged human HSP27 protein was robustly expressed in brain neurons of N-HSP27 mice (Fig. S1 *B* and *E*) and in cerebral microvascular ECs of EC-HSP27 mice (Fig. S1 *D* and *F*), respectively. In nonstroke brains, no significant difference was observed in the microvasculature of N-HSP27 and EC-HSP27 mice compared with WT mice, with respect to surface area and branch points (Fig. S1 *G* and *H*). When subjected to transient focal cerebral ischemia (tFCI), N-HSP27 and EC-HSP27 transgenic mice showed comparable reductions in cortical cerebral blood flow (CBF) as WT mice (Fig. 1 *A* and *B*), suggesting that HSP27 overexpression in either neurons or ECs does not affect the severity of the original ischemic insult.

To assess BBB permeability after tFCI, we analyzed the extravasation of blood components into the brain parenchyma, including i.v.-injected fluorescent tracer Alexa 555 cadaverine (0.95 kDa) and endogenous plasma IgG (~150 kDa). Consistent with our recent findings (9), tFCI induced progressive deterioration of BBB integrity in WT mice, manifested as the staggered leakage of small macromolecules followed by large macromolecules. Specifically, the extravasation of cadaverine was detected in both the ipsilateral cortex and striatum at 1 h after tFCI, whereas IgGs were seen in the same regions at 3 h after tFCI, the first time point examined after 1 h (Fig. 1*C* and Fig. S2). N-HSP27 and WT mice showed comparable volumes with visible leakage of cadaverine at 1–24 h after tFCI and of IgG at 3–24 h after tFCI (Fig. 1*D*). These data suggest that neuron-specific HSP27 overexpression does not protect against I/R-induced BBB disruption. In contrast, EC-HSP27 mice showed significantly reduced extravasation of both cadaverine (1–24 h after tFCI) and IgG (3–24 h after tFCI). Furthermore, brain regions with robust BBB breakdown at acute stages (1–3 h) after tFCI evolved into infarct zones at 24 h after tFCI (Fig. 1*C*, MAP2-negative areas). Although N-HSP27 mice had reduced infarct volumes at 24 h after tFCI compared with WT mice, this difference disappeared by 72 h after tFCI (Fig. 1 *E* and *F*). In contrast, EC-HSP27 mice showed significantly reduced infarct volumes at both 24 h ($P \leq 0.01$ vs. WT) and 72 h ($P \leq 0.01$ vs. WT; $P = 0.077$ vs. N-HSP27) after tFCI. In summary, these results suggest that EC-targeted overexpression of HSP27 not only ameliorates tFCI-induced BBB damage but also confers greater protection against ischemic infarction than neuron-specific overexpression.

EC-Targeted HSP27 Overexpression Improves Long-Term Stroke Outcomes. Next we investigated whether EC-targeted HSP27 overexpression leads to long-term functional improvements in stroke mice. Commonly used neurobehavioral tests for assessing neurological deficits of mice show different patterns and time course of spontaneous recovery in stroke animals (23–25). To comprehensively evaluate sensorimotor functions after stroke, a battery of four different behavioral tests was performed on WT, N-HSP27, and EC-HSP27 mice before and up to 21 d after tFCI (Fig. 2 *A*–*D*). In all groups of mice, tFCI induced motor deficiencies (rotarod and pole tests) and sensorimotor and postural asymmetries (cylinder and corner tests), and these deficits were the most prominent in the first week after tFCI. Over a 2- to 3-wk period after tFCI, all stroke groups experienced at least partial recovery in all four tests, and EC-HSP27, but not N-HSP27 mice, demonstrated superior functional recovery after tFCI compared with WT mice (Fig. 2 *A*–*D*; $P \leq 0.05$ or $P \leq 0.01$ by two-way ANOVA). Specifically, EC-HSP27 but not N-HSP27 mice performed significantly better than WT mice at earlier time points after stroke in the rotarod (day 5 and 7) and cylinder (day 3, 7, and 10) tests ($P \leq 0.05$ vs. WT by one-way ANOVA), whereas all three stroke groups (WT, N-HSP27, and EC-HSP27) recovered to comparable levels within 14–21 d after tFCI (Fig. 2 *A* and *C*; $P > 0.05$ between any two groups by one-way ANOVA). These results suggest that EC-targeted HSP27 overexpression facilitated spontaneous sensorimotor recovery after stroke, as demonstrated by the rotarod and cylinder tests. In contrast, WT mice showed relatively poorer long-term recovery (21 d after tFCI; Fig. 2 *B* and *D*) in the pole test and corner test; in both tests, EC-HSP27 but not N-HSP27 mice exhibited significant improvements in performance not only at earlier time points (day 5 and 7 in the pole test; day 7 and 9 in the corner test; $P \leq 0.05$ or $P \leq 0.01$ vs. WT by one-way ANOVA), but also at later time points (day 14 and 21, $P \leq 0.05$ or $P \leq 0.01$ vs. WT by one-way ANOVA) compared with WT mice, indicating that EC-targeted HSP27 overexpression enhanced overall sensorimotor recovery after stroke.

At 21 d after tFCI, all postischemic mice developed brain atrophy in the ipsilateral hemisphere (Fig. 2*E*). Consistent with the observed improvements in neurological functions, brain atrophy

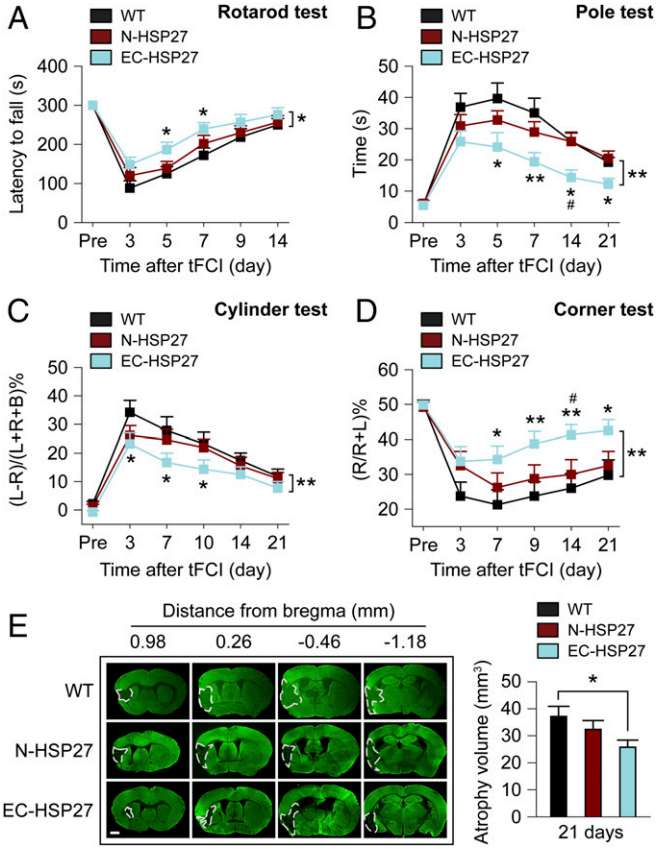

Fig. 2. EC-targeted overexpression of HSP27 improves long-term histological and functional outcomes after I/R brain injury. tFCI was induced for 1 h in WT mice, and in neuron- or EC-specific HSP27-overexpressing mice. (*A*–*D*) Sensorimotor deficits were assessed before (Pre) and up to 21 d after tFCI by a battery of behavioral tests. (*A*) Rotarod test. (*B*) Pole test. (*C*) Cylinder test. L, left; R, right; B, both forepaws. (*D*) Corner test. R, number of right turns (impaired side after occlusion of the left middle cerebral artery); L, number of left turns (nonimpaired side). (*E*) Tissue atrophy was measured at 21 d after tFCI on MAP2 (green)-stained coronal sections. Dashed line, brain infarct. $n = 8$ mice per group. (Scale bar: 1 mm.) $^{*}P \leq 0.05$, $^{**}P \leq 0.01$ EC-HSP27 vs. WT by one-way ANOVA (individual time point) or two-way ANOVA (bracket). $^{\#}P \leq 0.05$ EC-HSP27 vs. N-HSP27 by one-way ANOVA.

was significantly reduced in EC-HSP27 mice ($P \leq 0.05$), but not in N-HSP27 mice ($P = 0.12$), compared with WT mice. In summary, these results demonstrate that HSP27 overexpression targeted to ECs, but not to neurons, results in long-term functional and histological improvements in mice after tFCI. Although neuronal HSP27 overexpression offered acute protection against ischemic infarct (at 24 h after tFCI; Fig. 1*E*), its beneficial effects dissipated beyond the 24-h time window.

HSP27 Mitigates I/R-Induced BBB Permeability in an in Vitro Model. To investigate the mechanisms underlying BBB protection against I/R injury in endothelial HSP27-overexpressing mice, we established an in vitro BBB model consisting of a monolayer of human brain microvessel endothelial cells (HBMECs) in a Transwell culture insert (Fig. 3*A* and *SI Materials and Methods*). The system was subjected to the ischemia-like insult of oxygen–glucose deprivation (OGD) for 1 h, and the luminal-to-abluminal barrier permeability to fluorescent tracers of three different sizes was evaluated after 1–6 h of post-OGD reperfusion. Compared with non-OGD cultures, OGD and reperfusion induced progressive increases in barrier permeability, manifested as increased diffusion rate. In particular, the two small-size tracers (0.95 kDa cadaverine and 4.4 kDa dextran) crossed the EC barrier already at 1 h after OGD (Fig. S3 and Fig. 3 *B* and *C*), but the larger test molecule (70 kDa dextran) did not cross the EC layer during the first 3 h after OGD (Fig. 3*D*). At 4 and 6 h after OGD, the larger macromolecules also crossed the EC barrier; meanwhile, there was further increased leakage of the two small-size tracers across the barrier compared with the 3-h time point after OGD (Fig. S3 and Fig. 3 *B–D)*. When HSP27 was overexpressed in HBMECs by lentivirus-mediated transfection before OGD, the leakage of the small-size tracers was significantly reduced, but not prevented, at 1–6 h after OGD and of the large tracer at 4–6 h after OGD (Fig. 3 *B–D*). Thus, we confirmed that endothelial HSP27 significantly attenuated OGD-induced BBB leakage to both small- and large-size macromolecules in vitro, and used this HBMEC culture model for subsequent mechanistic studies.

One hour of OGD did not cause overt cell death in cultured HBMECs within the first 6 h of reperfusion (Fig. S4), suggesting that the HSP27-afforded attenuation of BBB leakage in vitro does not depend on its antiapoptotic properties.

HSP27 Inhibits OGD-Induced Actin Polymerization and Junctional Protein Redistribution in Cultured ECs. We recently reported that aberrant actin polymerization and the translocation of endothelial junctional proteins from the extracellular space to the cytosol are responsible for the increase in BBB permeability during the first 3 h after OGD, the evidence being that this loss of barrier function could be prevented by overexpression of actin depolymerizing factor (ADF), which inhibits actin polymerization, or knockdown of MLC (9). Previous studies demonstrated that HSP27 directly interacts with actin and is a potent inhibitor of actin polymerization (19, 20). Thus, we hypothesized that HSP27 may, like ADF, ameliorate BBB disruption by inhibiting the aberrant actin polymerization in ECs after OGD. Indeed, OGD rapidly enhanced actin polymerization in cultured HBMECs, as manifested by the robust formation of F-actin$^+$ stress fibers (Fig. 4*A* and Fig. S5) and by an increase in the ratio of F-actin to G-actin at 1 and 3 h after OGD (Fig. 4*B*). Lentivirus-mediated HSP27 overexpression significantly inhibited the F-actin$^+$ stress fiber formation and reduced the F/G-actin ratio to near control levels at 1 and 3 h after OGD (Fig. 4 *A* and *B*), thus confirming the role of HSP27 as an inhibitor of actin polymerization in post-OGD ECs.

We recently identified two signaling pathways that underlie actin polymerization and stress fiber formation in post-OGD ECs, i.e., phosphorylation/inactivation of ADF/cofilin and phosphorylation/activation of MLC, which promote actin polymerization and formation of stress fibers from short F-actins, respectively (9). To determine whether HSP27 affects either ADF/cofilin or MLC phosphorylation in ECs, HBMECs transfected with HSP27 or control vectors were subjected to OGD followed by 1 or 3 h of reperfusion. OGD markedly elevated the levels of both p-ADF/cofilin and p-MLC in HBMECs, whereas HSP27 overexpression did not modify the level of either phosphoprotein (Fig. S6). These results are in line with previous findings that HSP27 is a direct actin depolymerizing protein (19, 20).

Contractile stress fibers transmit tension to cell junctions that are anchored to the actin cytoskeleton and disassemble the junctional complexes (9, 11). At 1 h after OGD, the distribution of TJ proteins occludin and zona occludens (ZO)-1, as well as the AJ protein vascular endothelial (VE)-cadherin partially shifted from the membrane fraction to the actin cytoskeleton fraction (ACF), whereas total protein levels in whole-cell lysates remained unchanged (Fig. 4*C*). This protein translocation was greatly reduced when HSP27 was overexpressed in HBMECs. Immunocytochemical studies confirm the decreased levels of VE-cadherin and ZO-1 at their normal expression sites—the cell–cell contact zones—at 1 and 3 h after OGD compared with non-OGD conditions, and perinuclear immunofluorescence of VE-cadherin and ZO-1 was observed in some cells (Fig. 4 *D* and *E* and Fig. S5 *C* and *D*), consistent with the redistribution of these two junctional proteins after OGD. This effect was markedly attenuated in HBMECs overexpressing HSP27. On 3D plots showing fluorescence intensity on the *z* axis (Fig. 4*F*), we observed abundant VE-cadherin immunostaining surrounding the nucleus in some OGD-treated HBMECs. In contrast, VE-cadherin and nuclear signals were topographically separated under non-OGD conditions or with HSP27 overexpression (Fig. 4*F*).

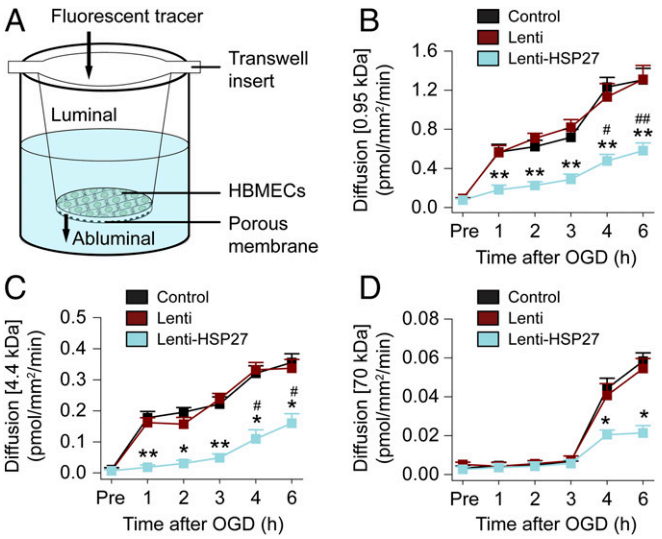

Fig. 3. Overexpression of HSP27 within ECs reduces BBB permeability after OGD in vitro. (*A*) Illustration of the in vitro BBB model. Cultured HBMECs were seeded on top of a membrane in the cell culture insert and grown for 4 d to form a confluent monolayer. HBMECs were infected for 72 h with empty lentivirus (Lenti), or lentiviral vectors carrying HA-tagged human HSP27 (Lenti-HSP27), and then subjected to an ischemia-like insult OGD for 1 h. Paracellular permeability was quantified at 1–6 h after OGD by the luminal to abluminal diffusion rate of three fluorescent tracers with different molecular weights. (*B–D*) Shown are the diffusion rates of the 0.95-kDa Alexa 555 cadaverine (*B*), the 4.4-kDa TRITC–dextran (*C*), or the 70-kDa FITC–dextran (*D*) before OGD (Pre) and at 1–6 h after OGD. Data represent the mean and SEM of four independent experiments. $^*P \leq 0.05$, $^{**}P \leq 0.01$ Lenti-HSP27 vs. Lenti. $^{\#}P \leq 0.05$, $^{\#\#}P \leq 0.01$ vs. Pre-OGD for Lenti-HSP27.

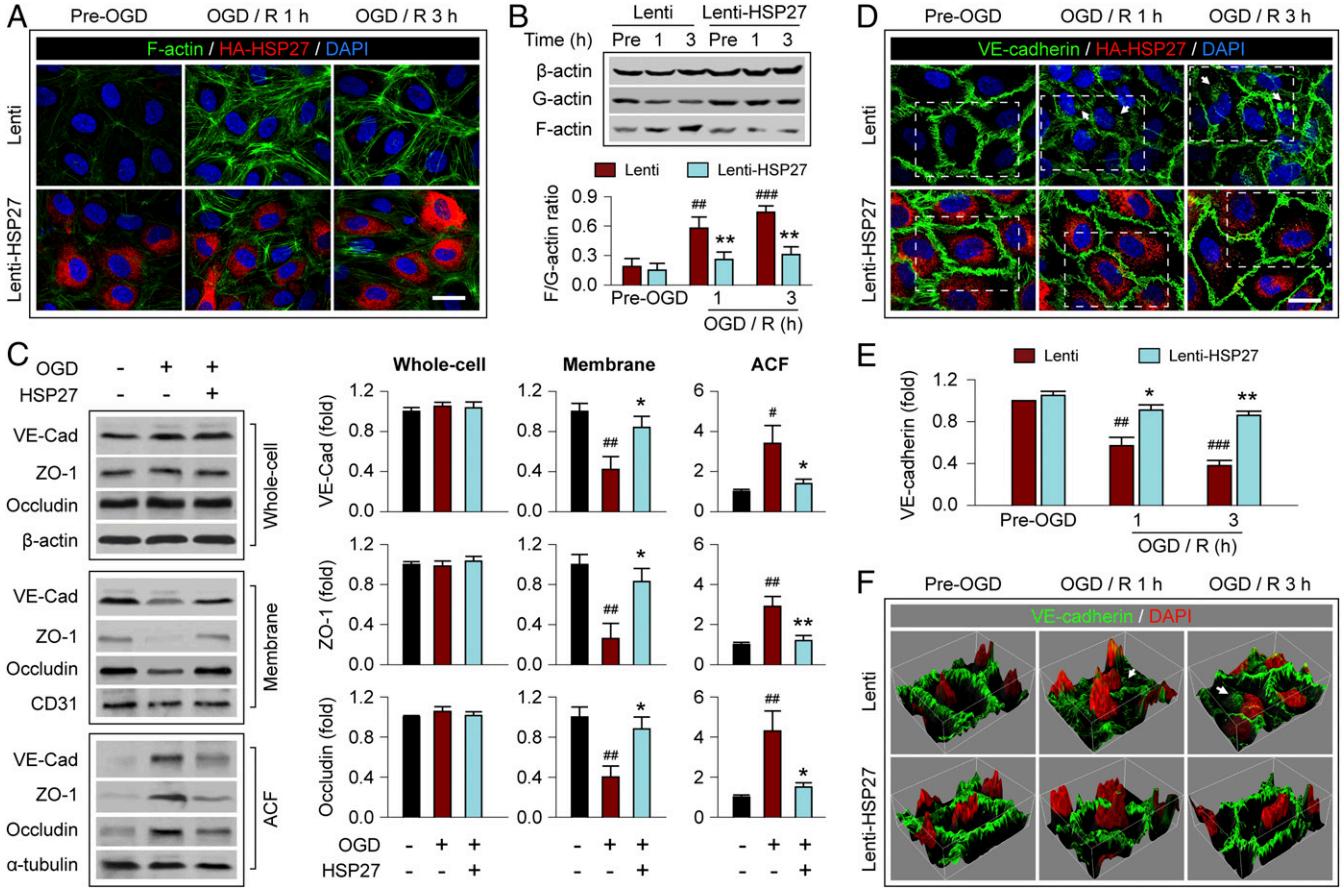

Fig. 4. Overexpression of HSP27 inhibits OGD-induced formation of stress fibers and translocation of junctional proteins in cultured ECs. Cultured HBMECs were transfected with Lenti or Lenti-HSP27. Seventy-two hours later, cells were subjected to 1 h of OGD, followed by 1 or 3 h of reperfusion (R). (*A*) Cells were triple-labeled for F-actin$^+$ stress fibers, HA-tagged HSP27, and the nuclear marker DAPI. OGD-induced stress fiber formation was markedly attenuated by HSP27 overexpression at both 1 and 3 h of reperfusion. (Scale bar: 30 μm.) (*B*) The expression of total β-actin, soluble G-actin, and polymerized F-actin in HBMECs was examined by Western blotting before OGD or at 1 and 3 h after OGD. The ratio of F-actin to G-actin was quantified as a measure of stress fiber formation; the ratio was increased by OGD/R but significantly less in Lenti-HSP27–transfected cells. (*C*) Whole-cell extract, the membrane fraction, or the ACF were prepared at 1 h after post-OGD reperfusion and immunoblotted for VE-cadherin (VE-Cad), ZO-1, occludin, and subfraction markers β-actin, CD31, or α-tubulin. Representative images and quantification of blots are presented. (*D*) HBMECs were stained for VE-cadherin, HA-tagged HSP27, and DAPI. HA-HSP27 distributes uniformly in the cytosol, and VE-cadherin is characteristically located at cell–cell appositions under physiological, uninjured conditions. OGD resulted in a loss of VE-cadherin from the appositions, and label was increased in the cytosol (arrow). This effect was inhibited by lentiviral HSP27 overexpression. Rectangles: regions that were used to construct the 3D plots in *F*. (Scale bar: 30 μm.) (*E*) The immunofluorescence of VE-cadherin at the cell–cell contacts was semiquantitatively measured, and data are expressed relative to pre-OGD controls. (*F*) 3D plots generated from the fluorescence of VE-cadherin and DAPI in *D*. The luminance of the fluorescence image was represented by height of the plot. Arrow: the cytosolic staining of VE-cadherin. Data in *B*, *C*, and *E* represent the mean and SEM of four independent experiments. $^*P \le 0.05$, $^{**}P \le 0.01$ Lenti-HSP27 vs. Lenti. $^{\#}P \le 0.05$, $^{\#\#}P \le 0.01$, $^{\#\#\#}P \le 0.001$ OGD/R vs. pre-OGD.

Endothelial HSP27 Overexpression Attenuates Stress Fiber Formation and Junctional Protein Redistribution in Brain Microvessels After tFCI. Thus far, we have demonstrated that endothelium-targeted HSP27 overexpression mitigated actin polymerization and redistribution of junctional proteins after OGD exposure in vitro. Therefore, we further examined the mechanism underlying BBB protection by HSP27 in vivo, using endothelial HSP27-overexpressing mice and WT mice subjected to tFCI and 1 or 3 h of reperfusion. Using confocal microscopy, F-actin$^+$ dense stress fibers, a hallmark of increased actin polymerization, were frequently detected in cortical microvessels of WT mice after tFCI, but only rarely observed in postischemic EC-HSP27 mice (Fig. 5*A*). Immunoblot analysis of protein extracts from purified cortical microvessels revealed that the percentage of F-actin over total actin was significantly elevated in the postischemic hemisphere at 1 h after tFCI compared with the contralateral nonischemic hemisphere in WT mice, and that this I/R-induced increase was attenuated in EC-HSP27 mice (Fig. 5*B*).

Results of subcellular fractionation of cortical microvessel extracts followed by immunoblotting revealed that the junctional proteins occludin, ZO-1, and VE-cadherin were partially but significantly redistributed from the membrane fraction to ACF at 1 h after tFCI (Fig. 5*C*), similar to that observed in HBMEC cultures after OGD (Fig. 4*C*). This tFCI-induced protein translocation was reduced in EC-HSP27 mice. Together, these data from in vitro and in vivo models support our hypothesis that HSP27 preserves BBB integrity after I/R by inhibiting actin polymerization and the barrier-destructive redistribution of junctional proteins in postischemic ECs.

EC-Targeted Overexpression of HSP27 Impedes the Infiltration of Peripheral Immune Cells After tFCI. Leukocytes that infiltrate through the impaired BBB play an important role in the development of permanent neurovascular injury and neurological deficits after I/R (26). Blood neutrophils and macrophages carry proinflammatory mediators into the brain, such as gelatinase

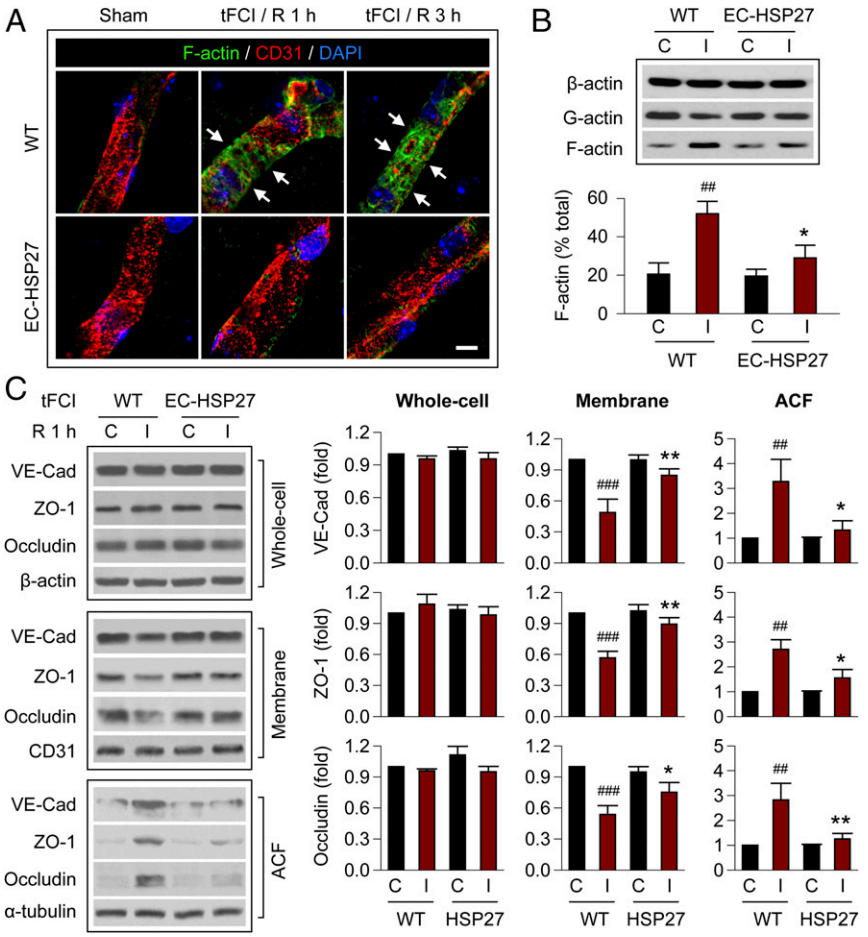

Fig. 5. EC-targeted HSP27 overexpression reduces stress fiber formation and translocation of junctional proteins in cerebral microvessels after tFCI. WT or EC-HSP27 mice were subjected to 1 h of tFCI or sham operation. (*A*) Representative images showing the formation of F-actin$^+$ stress fibers in CD31$^+$ microvessels (arrows) in the cortex of the ischemic hemisphere at 1 and 3 h after tFCI. (Scale bar: 10 μm.) Endothelial HSP27 overexpression inhibited tFCI-induced formation of stress fibers. (*B*) Brain microvessel extracts were collected from the contralateral (C) and ipsilateral (I) cortex at 1 h reperfusion after 1 h tFCI for Western blot analysis of total β-actin, G-actin, and F-actin. The content of F-actin was quantified as percentage of total β-actin. $n = 4$ mice per group. (*C*) Whole-cell extract, the membrane fraction, or the ACF was prepared from cortical microvessels at 1 h reperfusion after 1 h tFCI and subsequently immunoblotted. Representative images and quantification of blots (normalized to WT contralateral) are presented. Endothelial HSP27 overexpression suppressed tFCI-induced redistribution of junctional proteins VE-cadherin, ZO-1, and occludin from the membrane fraction to the ACF. $n = 4$–5 mice per group. $^*P \le 0.05$, $^{**}P \le 0.01$ EC-HSP27 vs. WT (ipsilateral hemisphere). $^{\#\#}P \le 0.01$, $^{\#\#\#}P \le 0.001$ ipsilateral vs. contralateral hemisphere.

B/MMP-9, causing further BBB damage and secondary expansion of ischemic injury (9, 27). We hypothesized that the preservation of BBB integrity by HSP27 blocks post-tFCI infiltration of immune cells, thereby improving long-term stroke outcomes. A flow cytometry-based strategy was used to quantitatively analyze the brain infiltration of leukocytes at 48 h after tFCI (Fig. S7). In WT mice, CD11b$^+$Ly6G$^+$ cells were dramatically increased in the post-tFCI brain hemisphere compared with sham-operated mice (Fig. 6 *A* and *B*), reflecting the robust infiltration of blood neutrophils (28) into the brain. In the Ly6G$^-$ cell population, tFCI also induced an increase in the number of CD11b$^+$CD45^{high} cells (representing infiltrated macrophages and activated microglia; Fig. 6 *A* and *B*). In contrast to WT mice, tFCI-induced brain infiltration of neutrophils and macrophages was significantly reduced in EC-HSP27 mice. These results were confirmed by immunohistochemistry in another cohort of mice, in which neutrophils and macrophages were immunolabeled for myeloperoxidase (MPO) and F4/80 (29, 30), respectively (Fig. 6*C*). Quantitatively, tFCI-induced increases in brain infiltration of MPO$^+$ and F4/80$^+$ cells were significantly smaller in EC-HSP27 mice compared with WT mice (Fig. 6*D*). To test whether the attenuation of neutrophil and macrophage infiltration alleviates the proinflammatory reactions in the postischemic brain, we measured a panel of inflammatory mediators in the ipsilateral brain hemisphere at 48 h after tFCI using the ChemiArray Mouse Antibody Array Kit. Indeed, of the nine inflammation markers that were elevated by tFCI in WT mice compared with sham controls, seven showed reduced expression in EC-HSP27 mice compared with WT mice (Fig. 6*E*).

Using the in vitro BBB model, we tested the effect of HSP27 overexpression on leukocyte transmigration across the endothelial barrier after OGD (Fig. S8*A*). Preexposure of HBMECs to OGD markedly enhanced the transmigration of neutrophil and macrophage across the barrier, whereas these changes were significantly attenuated in HBMEC cultures transfected with HSP27 (Fig. S8*B*). Taken together, these results support our hypothesis that HSP27 inhibits the brain infiltration of leukocytes and inflammatory responses after I/R by strengthening the endothelial barrier. Nevertheless, these experiments do not prove the mechanism by which HSP27 reduces the transmigration of neutrophils and macrophages across the barrier, because both of the paracellular and transcellular pathways have been hypothesized for such transmigration (31, 32). Because both pathways involve actin dynamics (32), whether HSP27 acts through either or both pathways warrants further investigation.

Post-tFCI Administration of TAT-HSP27 Alleviates BBB Disruption and Improves Long-Term Stroke Outcomes. Thus far, we had demonstrated that transgenic overexpression of human HSP27 in ECs is sufficient to attenuate I/R-induced BBB disruption and improve long-term stroke outcome. Next, we determined whether administration of a cell-penetrating recombinant HSP27 protein after the onset of reperfusion elevates HSP27 levels in brain ECs and protects against I/R-induced BBB disruption. To this end, a cell-penetrating HSP27 fusion protein containing the 11-aa protein transduction domain (PTD) derived from the HIV TAT protein was generated and purified (Fig. S9 *A* and *B*). Intravenous injection of TAT-HSP27, but not the HSP27 protein without the PTD, resulted in widespread delivery of HSP27 into

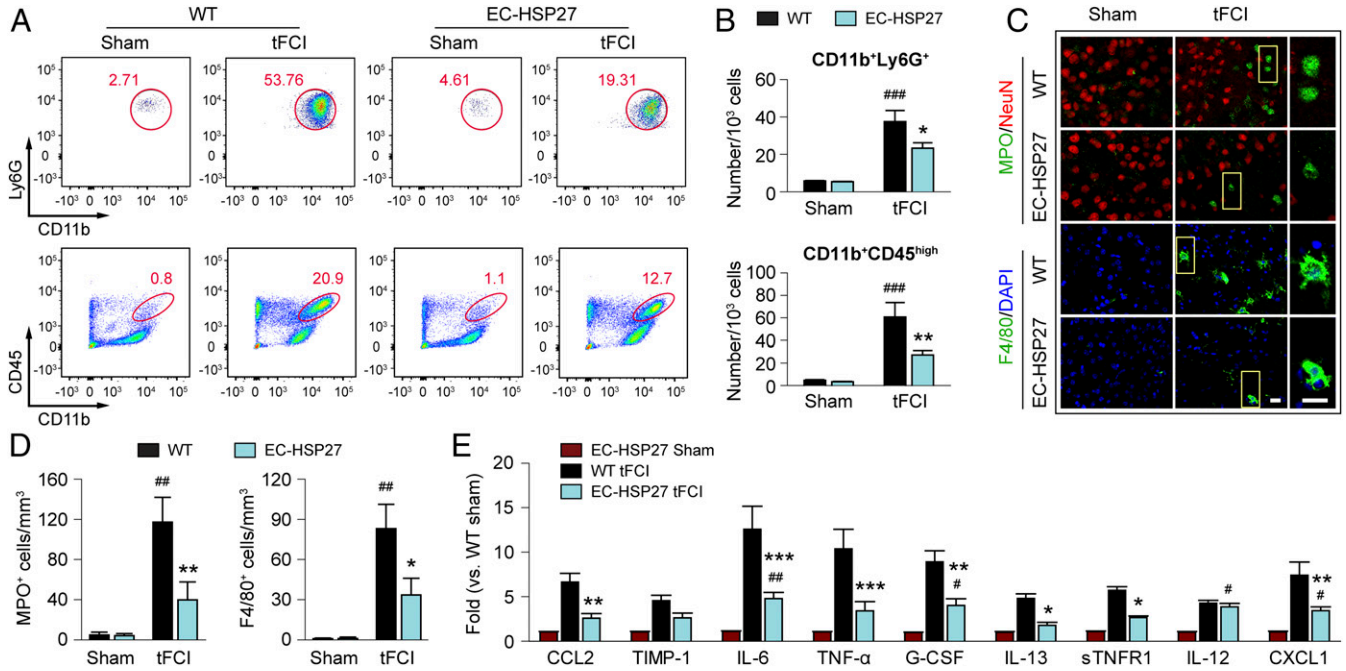

Fig. 6. EC-targeted HSP27 overexpression reduces the infiltration of peripheral immune cells after tFCI. WT or EC-HSP27 mice were subjected to sham operation or 1 h of tFCI followed by 48 h of reperfusion. (*A* and *B*) Cell suspensions were prepared from the ipsilateral hemispheres and flow cytometry was performed to quantify $Ly6G^+$ (infiltrated neutrophils) and $CD45^{high}$ (macrophages and activated microglia) cells among the $CD11b^+$ cell populations. (*A*) Representative density plots. (*Upper*) $CD11b^+Ly6G^+$ cells (circle) gated from total single cells. Numbers shown are the percentage of circled cells to total single cells (Fig. S7, G1 events). (*Lower*) $CD11b^+CD45^{high}$ cells (ovals) gated from the $Ly6G^-$ cell population. Numbers shown are the percentage of cells in each oval to total $Ly6G^-$ cells (Fig. S7, G4 events). (*B*) Cells were quantified and presented as the number of cells per 10^3 single cells. $n = 4$ mice for WT sham, $n = 9$ mice for EC-HSP27 sham, $n = 6$ mice for WT and EC-HSP27 tFCI. $^*P \le 0.05$, $^{**}P \le 0.01$ vs. WT. $^{\#\#\#}P \le 0.001$ vs. sham. (*C*) Representative images taken from the ipsilateral periinfarct cortex after tFCI or the corresponding region after sham operation, showing immunofluorescence of the following markers: MPO (neutrophil), F4/80 (macrophage), and NeuN (neuron). Rectangle: the region enlarged in high-power images (third column). (Scale bar: 20 μm.) (*D*) MPO^+ and $F4/80^+$ cells were counted in the areas described in *C* and data expressed as the number of cells per mm^3. $n = 4$ mice per group for sham. $n = 7$–8 mice per group for tFCI. MPO^+ and $F4/80^+$ cells were increased more in WT than in EC-HSP27 mice. $^*P \le 0.05$, $^{**}P \le 0.01$ vs. WT. $^{\#\#}P \le 0.01$ vs. sham. (*E*) A panel of inflammation markers was measured in the ipsilateral hemisphere at 48 h after tFCI (*SI Materials and Methods*). Shown are nine markers that were significantly increased ($P \le 0.05$) in the WT brains after tFCI compared with WT sham controls among the total 32 markers tested. $n = 4$ mice per group for sham. $n = 5$ mice per group for tFCI. $^*P \le 0.05$, $^{**}P \le 0.01$, $^{***}P \le 0.001$ EC-HSP27 tFCI vs. WT tFCI. $^{\#}P \le 0.05$, $^{\#\#}P \le 0.01$ EC-HSP27 tFCI vs. EC-HSP27 sham.

brain microvascular endothelium within 1 h after injection (Fig. S9 *C*–*E*). When administered at 10 min, 2 h, and 24 h after tFCI, TAT-HSP27 effectively reduced the blood-to-brain leakage of Alexa 555 cadaverine and plasma IgG at 1, 3, and 24 h after tFCI, compared with mice treated with the control HSP27 protein (Fig. 7*A*). This amelioration of BBB disruption was manifested by a reduction in the amount of tracers found in the regions with BBB leakage (shown by decreased fluorescent intensity of cadaverine on surface plot images; Fig. 7*B*), as well as a reduction in the volume of brain showing leakage of cadaverine and of IgG (Fig. 7*C*). In separate cohorts of mice, post-tFCI administration of TAT-HSP27 significantly improved long-term sensorimotor (adhesive removal test; Fig. 7*D*) and spatial learning and memory (Morris water maze; Fig. 7*E*) functions of poststroke mice. Together with these improvements in neurological function, TAT-HSP27 treatment also reduced the acute ischemic infarct formed at 24 h after tFCI and the development of brain atrophy determined at 35 d after tFCI (Fig. 7*F*). Collectively, these data demonstrate that the cell-penetrating TAT-HSP27, when delivered at 10 min, 2 h, and 24 h after onset of reperfusion, is effective not only in preserving BBB integrity but also conferring prolonged protection against neurovascular injury and impairment of brain functions.

Discussion

The present study investigated the protective role of endothelium-targeted overexpression of HSP27 against BBB damage in a rodent model of brain I/R (Fig. 8). The results demonstrate that HSP27 overexpression in ECs attenuates I/R-induced early onset BBB disruption, presumably by inhibiting actin polymerization and the formation of force-generating, contractile stress fibers that lead to translocation of TJ and AJ proteins. By preserving BBB integrity after I/R, HSP27 reduces the recruitment of tissue destructive circulating neutrophils and macrophages into the brain parenchyma, thereby eliciting long-term protection against neurological deficits. The results also provide preclinical evidence that post-I/R administration of a cell membrane-permeable HSP27 fusion protein is effective in ameliorating BBB damage and improving long-term stroke outcome.

HSP27 is a unique stress-responsive protein that can serve as a dynamic signaling molecule under various insults (14). For example, HSP27 can inhibit apoptosis by reducing caspase activity (33), decrease cytochrome *c* release from mitochondria (34), and/or inactivate the apoptosis signal-regulating kinase 1/JNK prodeath signaling cascade (17). A number of previous studies reported the neuroprotective effects of HSP27 against cerebral I/R injury when globally expressed in the brain (15–17, 22). However, the anti-cell death properties of HSP27 are unlikely to directly contribute to protection against BBB leakage 1–3 h after I/R, because cell death is not apparent until some hours after this early stage in postischemic ECs (Fig. S4). Moreover, the expression of endogenous HSP27 is induced in postischemic brain mainly in nonneuronal cells, glia (18) as well as ECs (22), raising the possibility that HSP27 works through additional mechanisms.

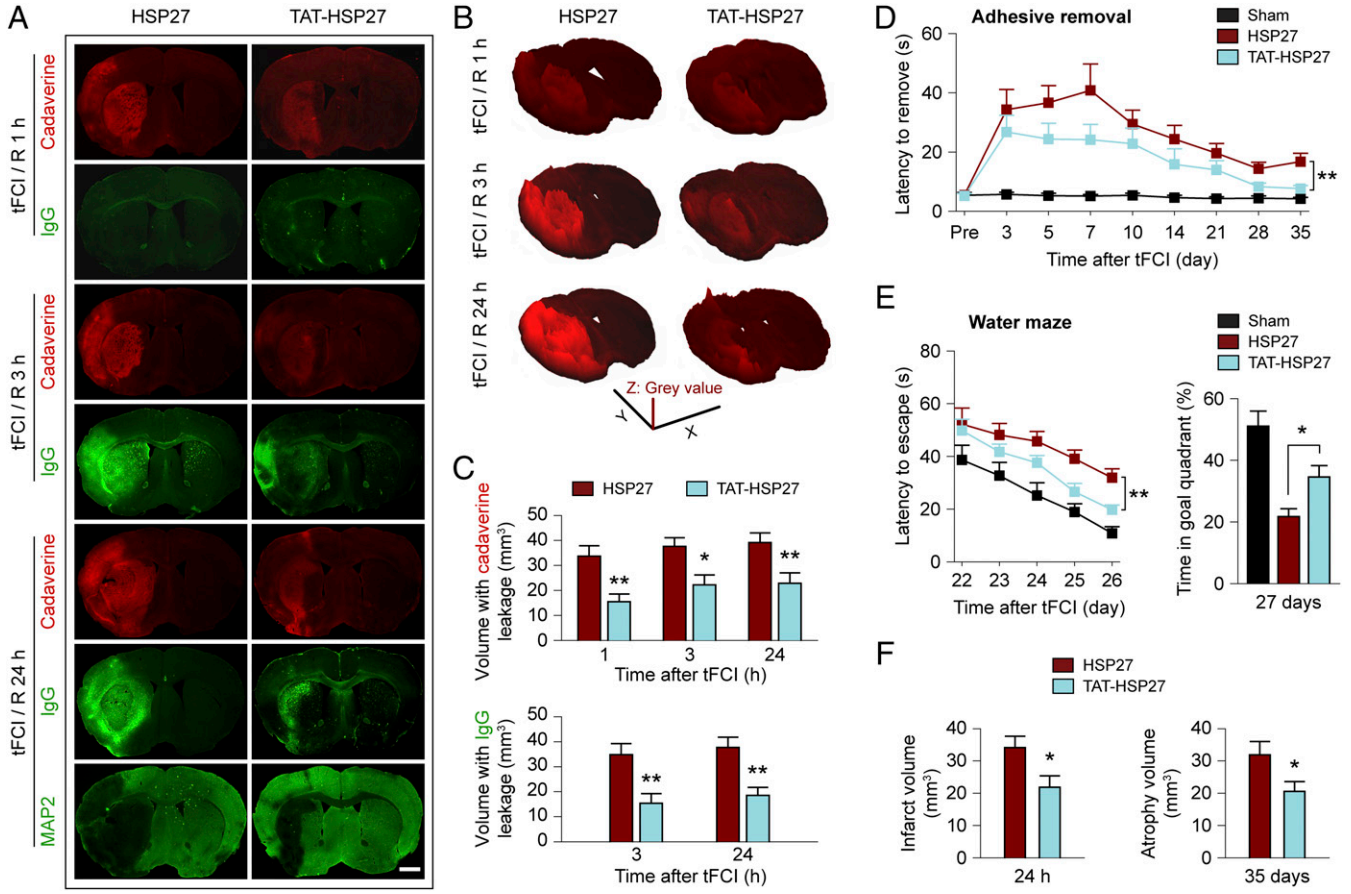

Fig. 7. Delivery of cell-penetrating TAT-HSP27 after tFCI ameliorates BBB impairment and improves functional outcomes. tFCI was induced in WT mice for 1 h followed by reperfusion. For each animal, TAT-HSP27 or control HSP27 protein (without the TAT domain) was administered at 10 min, 2 h, and 24 h after reperfusion was begun. (*A*) Representative images demonstrate the extravasation of Alexa 555 cadaverine or endogenous plasma IgG into the brain parenchyma 1, 3, or 24 h after tFCI. At 24 h after tFCI, MAP2 immunofluorescence on adjacent sections illustrates infarcts in the same brains. (Scale bar: 1 mm.) (*B*) 3D plots of brain coronal sections generated from the fluorescence of cadaverine in *A*, using luminance as height of the plot. (*C*) Brain volume showing leakage of cadaverine and IgG at indicated times of reperfusion after tFCI. $n = 5$–7 mice per group. (*D*) Sensorimotor functions were assessed up to 35 d after tFCI using the adhesive removal test. (*E*) Spatial cognitive functions were assessed at 22–27 d after tFCI by the Morris water maze. $n = 8$ mice per group. (*F*) Brain infarct volume at 24 h after tFCI, and chronic tissue atrophy at 35 d after tFCI were measured on MAP2-stained coronal sections. $n = 6$–7 mice per group for the 24-h measurement; $n = 8$ mice per group for the 35-d measurement. $^*P \leq 0.05$, $^{**}P \leq 0.01$ TAT-HSP27 vs. HSP27.

Our results show that HSP27 overexpression specifically targeted to ECs not only reduces I/R-induced BBB disruption but also leads to long-term parenchymal protection and superior neurological outcomes. In contrast, neuronal overexpression of HSP27 fails to reduce I/R-induced BBB disruption or prevent parenchymal damage beyond the 24-h time point after tFCI (Figs. 1 and 2). These observations suggest that the nonneuronal actions of HSP27 in ECs contribute to its overall protective effects against I/R injury.

Two important features of brain ECs, including the high sealing efficiency via paracellular junctions and relatively low transcytosis rate, help maintain the low permeability of the BBB to cerebrospinal fluid and blood components (35). Soon after I/R, there are increases in transcellular trafficking and paracellular permeability via MMP-independent mechanisms (8, 9). Transcellular efflux is increased as early as 6 h after I/R (8) and promotes caveolin-1–dependent transcytosis of blood albumin across the endothelial barrier. However, in the paracellular pathway of BBB disruption, which begins much earlier (at 0.5–1 h) after I/R (ref. 9 and present study), the aberrant subcellular redistribution of TJ proteins markedly reduces the EC sealing efficacy (and movement of AJ proteins may contribute), thus allowing the passage of proinflammatory macromolecules of small sizes (≤3 kDa) from blood to brain and, likely, from brain to blood across the barrier as well. HSP27 may inhibit the paracellular pathway of BBB impairment by preventing the endothelial subcellular redistribution of TJ and, possibly, AJ proteins after I/R injury. It remains to be determined whether HSP27 also affects the transcellular pathway of BBB disruption, although a recent study does not support an important role for this pathway in the I/R model used here (9).

The present findings show that HSP27 blocks aberrant actin polymerization and stress fiber formation in ECs, the putative driving force behind opening of the paracellular pathway for early BBB disruption after I/R. A cortical actin rim is formed in ECs under physiological conditions, serving as an important anchor for cell–cell and cell–matrix adhesions (36). Fluid shear stress experienced by quiescent ECs provides chronic mild stimulation toward the formation of stress fibers, which may interrupt the cortical actin network and break intercellular junctions through centripetal tension when homeostasis is disrupted (11, 37). It is well established that HSP27 directly inhibits actin polymerization by capping the barbed end of actin (20), where rapid addition of actin monomers occurs. Additionally, HSP27 can sequester G-actin monomers (21). As a consequence of either action, G-actin cannot bind to the plus end of F-actin and be further aggregated by myosin to form contractile stress fibers.

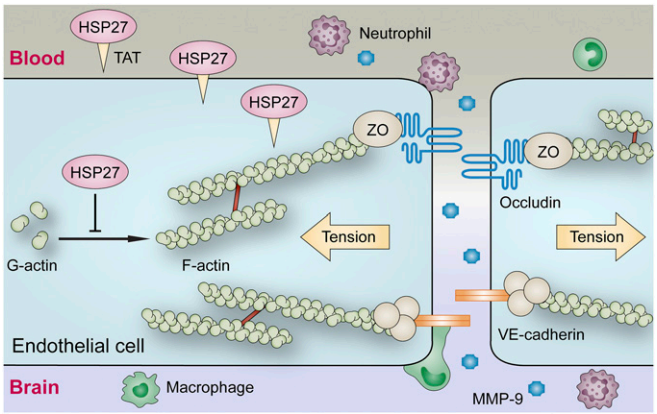

Fig. 8. Proposed mechanisms underlying HSP27-afforded protection of the BBB after cerebral I/R injury. HSP27 robustly inhibits I/R-induced actin polymerization and stress fiber formation in brain microvascular ECs, which reduces cellular tension from stress fibers that may cause disassembly and internalization of junctional proteins. After I/R, translocation of TJ and AJ proteins from cell–cell contacts to the cytosol opens the BBB and increases paracellular permeability to small macromolecules (less than 3 kDa). Subsequently, permeability to larger molecules increases. By fortifying the BBB, HSP27 blocks the infiltration of peripheral immune cells (not shown to scale) and reduces secondary brain injury, leading to sustained improvements in histological and neurological outcomes. Intravenous administration of a cell-penetrating TAT-HSP27 fusion protein results in rapid uptake of HSP27 into ECs and exerts similar protection as transgenic HSP27 overexpression against I/R-induced neurovascular injury.

Endogenous actin regulatory proteins, such as ADF/cofilin, play an important role in balancing actin polymerization and depolymerization processes, thus preventing excessive formation of stress fibers (38). Soon after cerebral I/R, endothelial ADF/cofilin is phosphorylated at serine 3, becoming disabled (9). Meanwhile, the RhoA/ROCK signaling pathway is activated, which may further promote the aggregation and cross-linking of F-actin into force-generating linear stress fibers through the phosphorylation/activation of MLC (9, 11, 36, 39). Our data presented here show that HSP27 attenuates I/R-induced actin polymerization and stress fiber formation, but without influencing the phosphorylation of either ADF/cofilin or MLC (Fig. S6). These results are consistent with previous findings that HSP27 is a direct inhibitor of actin polymerization (20, 21).

Why does the attenuation of early BBB disruption by HSP27 lead to long-term brain protection against I/R injury? Our results demonstrate that EC-HSP27 reduces the infiltration of neutrophils and macrophages into the postischemic brain parenchyma after tFCI (Fig. 6). The fortified BBB may directly block the transmigration of these cells from blood to brain, or reduce the efflux of inflammatory signals from brain to blood that recruit the blood cells. These infiltrating reactive immune cells may contribute to the development of permanent neurovascular injury via at least three distinctive yet interrelated mechanisms. First, leukocytes are the main source of MMP-9 production in the brain after I/R (40), although several components of the postischemic neurovascular unit (ECs, neurons, and microglia) can also release MMP-9 (41). Whereas I/R-induced early BBB disruption (less than 3 h of postischemic reperfusion) does not require MMPs per se, MMP-9 contributes to the secondary BBB breakdown 3–24 h after I/R by degrading the junctional complexes and basal lamina (9). The widening of EC paracellular space appears to provide a breakthrough point that allows leukocyte-derived MMPs to gain access to their proteolytic cleavage sites on TJ and AJ protein (9). Second, the infiltrating peripheral immune cells may aggravate the proinflammatory responses of the postischemic brain, because many of the overproduced cytokines and reactive oxygen or nitrogen species are tissue destructive. Indeed, our results revealed that endothelial HSP27 overexpression not only decreases leukocyte infiltration but also attenuates the otherwise marked elevations in multiple cytokines after I/R (Fig. 6). Third, the excessive infiltration of peripheral immune cells into the postischemic brain may produce an unfavorable microenvironment that hinders brain repair processes. However, it is widely accepted that neurovascular remodeling may be facilitated by infiltrated leukocytes during the poststroke recovery phase (26). Thus, a complete blockage of immune cell infiltration could be harmful for brain recovery. In the present study, post-I/R immune cell infiltration was attenuated, but not completely blocked, in EC-HSP27 mice (Fig. 6); this may balance the harmful vs. beneficial actions of leukocytes. Together, the early microarchitectural changes in ECs that disrupt the BBB serve as a starting point for a vicious feedforward cycle in which infiltration of tissue-destructive peripheral immune cells recruits further cells, eventually culminating in progressive and irreversible neurovascular injury. By protecting against early BBB disruption, HSP27 prevents initiation of such a vicious cycle, thereby preventing secondary injury.

Proof-of-concept experiments were performed to test the efficacy of administration of a cell-permeable HSP27 protein against I/R injury. Intravenous injection of TAT-HSP27 resulted in rapid delivery of the protein into cerebral ECs, and led to not only early BBB protection but also long-term improvement of histological and functional stroke outcomes. These results hold translational potential from the perspective of developing an effective therapy for I/R brain injury. However, the TAT protein transduction domain does not show cell type specificity in facilitating protein delivery. It has been shown that TAT fusion protein can be delivered into the brain parenchyma within 4 h after systemic injection of the protein (42). Accordingly, our data cannot exclude the potential non-BBB effects of TAT-HSP27 that could contribute to its long-term efficacy against I/R injury (or lead to side effects in brain or other tissues). Further, it is unknown whether this treatment is effective after relatively prolonged cerebral ischemia, because a reperfusion event usually occurs 2–4 h after ischemic stroke in the clinic, such as in patients who receive tPA thrombolytic therapy. Nevertheless, future research is warranted to test the effect of TAT-HSP27 in stroke models that encompass tPA-induced reperfusion and also to determine the time window of efficacy of this therapeutic strategy.

In conclusion, the present study demonstrates profound BBB protection by endothelium-targeted overexpression of HSP27 after I/R brain injury. TAT-HSP27 should be further explored as a treatment for ischemic stroke, especially in conjunction with recanalization therapy.

Materials and Methods

Animals. Transgenic mice that overexpress human HSP27 specifically in neurons were generated at the University of Pittsburgh Transgenic Core Facility. HSP27^{stop} transgenic mice for conditional overexpression of HSP27 were generated at the Shanghai Research Center for Model Organisms (Shanghai, China) through a service contract. To obtain mice with EC-targeted overexpression of HSP27, HSP27^{stop} mice were crossed with Tek-Cre mice (43), in which the Cre-mediated recombination is restricted to ECs. C57BL/6J mice were used as matched WT controls. All animal procedures were approved by the University of Pittsburgh Institutional Animal Care and Use Committee and performed in accordance with the NIH *Guide for the Care and Use of Laboratory Animals* (44). All efforts were made to minimize animal suffering and the number of animals used.

Transient Focal Cerebral Ischemia Model. tFCI was induced for 1 h in adult male mice (8–10 wk old, 25–30 g) by intraluminal occlusion of the left middle cerebral artery (MCAO) (9). Surgeries and all outcome assessments were performed by investigators blinded to mouse genotype and experimental group assignments.

Assessment of BBB Impairment After tFCI. BBB permeability was assessed by measuring the extravasation of an i.v.-injected fluorescent tracer (Alexa 555 cadaverine) and endogenous plasma IgG into the brain parenchyma. Coronal

brain sections were processed for direct fluorescence detection of Alexa 555, or subjected to immunofluorescent labeling of IgG and detection. The brain volume with cadaverine or IgG leakage was calculated on six equally spaced brain sections encompassing the MCA territory (9).

In Vitro BBB Model. Primary HBMECs were purchased from Cell Systems (ACBRI 376). The in vitro BBB model was established in cell culture inserts (9). To model ischemia in vitro, HBMECs were exposed to 1 h of OGD (17). Fluorescent tracers were added into the luminal chamber, and the diffusion rate of tracers from the luminal to the abluminal chamber was measured (9).

Statistical Analyses. Data are presented as mean ± SEM. Statistical comparison of the means between two groups was accomplished by Student's *t* test (two-tailed). Differences in means among multiple groups were analyzed using one- or two-way ANOVA followed by a Bonferroni/Dunn post hoc correction. A *P* value less than 0.05 was deemed statistically significant.

ACKNOWLEDGMENTS. This project was supported by US Department of Veterans Affairs (VA) Merit Review BX002495 (to J.C.); NIH Grants NS089534, NS045048, and NS056118 (to J.C.) and NS036736 and NS095029 (to M.V.L.B. and J.C.); Chinese Natural Science Foundation Grant 81571285 (to Y.G.); the Shanghai Municipal Science and Technology Commission Support Program 14431907002 (to Y.G.); and American Heart Association Grant 15POST22260011 (to Y.S.). J.C. is the Richard King Mellon Professor of Neurology and a recipient of the VA Senior Research Career Scientist Award. M.V.L.B. is the Sylvia and Robert S. Olnick Professor of Neuroscience and a recipient of the High-End Distinguished Professorship GDW20133100069 from the State Administration of Foreign Experts Affairs, China.

1. Obermeier B, Daneman R, Ransohoff RM (2013) Development, maintenance and disruption of the blood-brain barrier. *Nat Med* 19(12):1584–1596.
2. Khatri R, McKinney AM, Swenson B, Janardhan V (2012) Blood-brain barrier, reperfusion injury, and hemorrhagic transformation in acute ischemic stroke. *Neurology* 79(13, Suppl 1):S52–S57.
3. Moskowitz MA, Lo EH, Iadecola C (2010) The science of stroke: Mechanisms in search of treatments. *Neuron* 67(2):181–198.
4. Asahi M, et al. (2001) Effects of matrix metalloproteinase-9 gene knock-out on the proteolysis of blood-brain barrier and white matter components after cerebral ischemia. *J Neurosci* 21(19):7724–7732.
5. Liu J, Jin X, Liu KJ, Liu W (2012) Matrix metalloproteinase-2-mediated occludin degradation and caveolin-1-mediated claudin-5 redistribution contribute to blood-brain barrier damage in early ischemic stroke stage. *J Neurosci* 32(9):3044–3057.
6. Yang Y, Estrada EY, Thompson JF, Liu W, Rosenberg GA (2007) Matrix metalloproteinase-mediated disruption of tight junction proteins in cerebral vessels is reversed by synthetic matrix metalloproteinase inhibitor in focal ischemia in rat. *J Cereb Blood Flow Metab* 27(4):697–709.
7. Krueger M, et al. (2015) Blood-brain barrier breakdown involves four distinct stages of vascular damage in various models of experimental focal cerebral ischemia. *J Cereb Blood Flow Metab* 35(2):292–303.
8. Knowland D, et al. (2014) Stepwise recruitment of transcellular and paracellular pathways underlies blood-brain barrier breakdown in stroke. *Neuron* 82(3):603–617.
9. Shi Y, et al. (2016) Rapid endothelial cytoskeletal reorganization enables early blood-brain barrier disruption and long-term ischaemic reperfusion brain injury. *Nat Commun* 7:10523.
10. Krueger M, Härtig W, Reichenbach A, Bechmann I, Michalski D (2013) Blood-brain barrier breakdown after embolic stroke in rats occurs without ultrastructural evidence for disrupting tight junctions. *PLoS One* 8(2):e56419.
11. Burridge K, Wittchen ES (2013) The tension mounts: Stress fibers as force-generating mechanotransducers. *J Cell Biol* 200(1):9–19.
12. Stamatovic SM, Keep RF, Wang MM, Jankovic I, Andjelkovic AV (2009) Caveolae-mediated internalization of occludin and claudin-5 during CCL2-induced tight junction remodeling in brain endothelial cells. *J Biol Chem* 284(28):19053–19066.
13. Vandenbroucke E, Mehta D, Minshall R, Malik AB (2008) Regulation of endothelial junctional permeability. *Ann N Y Acad Sci* 1123:134–145.
14. Stetler RA, et al. (2010) Heat shock proteins: Cellular and molecular mechanisms in the central nervous system. *Prog Neurobiol* 92(2):184–211.
15. An JJ, et al. (2008) Transduced human PEP-1-heat shock protein 27 efficiently protects against brain ischemic insult. *FEBS J* 275(6):1296–1308.
16. Badin RA, et al. (2006) Neuroprotective effects of virally delivered HSPs in experimental stroke. *J Cereb Blood Flow Metab* 26(3):371–381.
17. Stetler RA, et al. (2008) Hsp27 protects against ischemic brain injury via attenuation of a novel stress-response cascade upstream of mitochondrial cell death signaling. *J Neurosci* 28(49):13038–13055.
18. Stetler RA, et al. (2012) Phosphorylation of HSP27 by protein kinase D is essential for mediating neuroprotection against ischemic neuronal injury. *J Neurosci* 32(8): 2667–2682.
19. Miron T, Wilchek M, Geiger B (1988) Characterization of an inhibitor of actin polymerization in vinculin-rich fraction of turkey gizzard smooth muscle. *Eur J Biochem* 178(2):543–553.
20. Miron T, Vancompernolle K, Vandekerckhove J, Wilchek M, Geiger B (1991) A 25-kD inhibitor of actin polymerization is a low molecular mass heat shock protein. *J Cell Biol* 114(2):255–261.
21. During RL, et al. (2007) Anthrax lethal toxin paralyzes actin-based motility by blocking Hsp27 phosphorylation. *EMBO J* 26(9):2240–2250.
22. Leak RK, et al. (2013) HSP27 protects the blood-brain barrier against ischemia-induced loss of integrity. *CNS Neurol Disord Drug Targets* 12(3):325–337.
23. Boltze J, Lukomska B, Jolkkonen J; MEMS–IRBI Consortium (2014) Mesenchymal stromal cells in stroke: Improvement of motor recovery or functional compensation? *J Cereb Blood Flow Metab* 34(8):1420–1421.
24. Balkaya M, Kröber J, Gertz K, Peruzzaro S, Endres M (2013) Characterization of long-term functional outcome in a murine model of mild brain ischemia. *J Neurosci Methods* 213(2):179–187.
25. Bouët V, et al. (2007) Sensorimotor and cognitive deficits after transient middle cerebral artery occlusion in the mouse. *Exp Neurol* 203(2):555–567.
26. An C, et al. (2014) Molecular dialogs between the ischemic brain and the peripheral immune system: Dualistic roles in injury and repair. *Prog Neurobiol* 115:6–24.
27. Justicia C, et al. (2003) Neutrophil infiltration increases matrix metalloproteinase-9 in the ischemic brain after occlusion/reperfusion of the middle cerebral artery in rats. *J Cereb Blood Flow Metab* 23(12):1430–1440.
28. Daley JM, Thomay AA, Connolly MD, Reichner JS, Albina JE (2008) Use of Ly6G-specific monoclonal antibody to deplete neutrophils in mice. *J Leukoc Biol* 83(1):64–70.
29. van Leeuwen M, et al. (2008) Accumulation of myeloperoxidase-positive neutrophils in atherosclerotic lesions in LDLR$^{-/-}$ mice. *Arterioscler Thromb Vasc Biol* 28(1):84–89.
30. Greter M, Lelios I, Croxford AL (2015) Microglia versus myeloid cell nomenclature during brain inflammation. *Front Immunol* 6:249.
31. Nourshargh S, Hordijk PL, Sixt M (2010) Breaching multiple barriers: Leukocyte motility through venular walls and the interstitium. *Nat Rev Mol Cell Biol* 11(5):366–378.
32. Schnoor M (2015) Endothelial actin-binding proteins and actin dynamics in leukocyte transendothelial migration. *J Immunol* 194(8):3535–3541.
33. Voss OH, et al. (2007) Binding of caspase-3 prodomain to heat shock protein 27 regulates monocyte apoptosis by inhibiting caspase-3 proteolytic activation. *J Biol Chem* 282(34):25088–25099.
34. Bruey JM, et al. (2000) Hsp27 negatively regulates cell death by interacting with cytochrome c. *Nat Cell Biol* 2(9):645–652.
35. Ben-Zvi A, et al. (2014) Mfsd2a is critical for the formation and function of the blood-brain barrier. *Nature* 509(7501):507–511.
36. Prasain N, Stevens T (2009) The actin cytoskeleton in endothelial cell phenotypes. *Microvasc Res* 77(1):53–63.
37. Franke RP, et al. (1984) Induction of human vascular endothelial stress fibres by fluid shear stress. *Nature* 307(5952):648–649.
38. Bamburg JR (1999) Proteins of the ADF/cofilin family: Essential regulators of actin dynamics. *Annu Rev Cell Dev Biol* 15:185–230.
39. Ridley AJ, Hall A (1992) The small GTP-binding protein rho regulates the assembly of focal adhesions and actin stress fibers in response to growth factors. *Cell* 70(3):389–399.
40. Li P, et al. (2013) Adoptive regulatory T-cell therapy protects against cerebral ischemia. *Ann Neurol* 74(3):458–471.
41. Rosell A, et al. (2006) Increased brain expression of matrix metalloproteinase-9 after ischemic and hemorrhagic human stroke. *Stroke* 37(6):1399–1406.
42. Cao G, et al. (2002) In vivo delivery of a Bcl-xL fusion protein containing the TAT protein transduction domain protects against ischemic brain injury and neuronal apoptosis. *J Neurosci* 22(13):5423–5431.
43. Koni PA, et al. (2001) Conditional vascular cell adhesion molecule 1 deletion in mice: Impaired lymphocyte migration to bone marrow. *J Exp Med* 193(6):741–754.
44. Committee on Care and Use of Laboratory Animals (1996) *Guide for the Care and Use of Laboratory Animals* (Natl Inst Health, Bethesda), DHHS Publ No (NIH) 85-23.
45. Fisher M, et al.; STAIR Group (2009) Update of the stroke therapy academic industry roundtable preclinical recommendations. *Stroke* 40(6):2244–2250.
46. Gan Y, et al. (2012) Transgenic overexpression of peroxiredoxin-2 attenuates ischemic neuronal injury via suppression of a redox-sensitive pro-death signaling pathway. *Antioxid Redox Signal* 17(5):719–732.
47. Zhang L, et al. (2002) A test for detecting long-term sensorimotor dysfunction in the mouse after focal cerebral ischemia. *J Neurosci Methods* 117(2):207–214.
48. Wang J, et al. (2014) Omega-3 polyunsaturated fatty acids enhance cerebral angiogenesis and provide long-term protection after stroke. *Neurobiol Dis* 68:91–103.
49. Cao G, et al. (2001) Intracellular Bax translocation after transient cerebral ischemia: Implications for a role of the mitochondrial apoptotic signaling pathway in ischemic neuronal death. *J Cereb Blood Flow Metab* 21(4):321–333.
50. Yin KJ, et al. (2010) Peroxisome proliferator-activated receptor delta regulation of miR-15a in ischemia-induced cerebral vascular endothelial injury. *J Neurosci* 30(18):6398–6408.